JOURNAL OF MATERIALS SCIENCE 32 (1997) 1603–1611

# An electron metallographic study of pressure die-cast commercial zinc–aluminium-based alloy ZA27

M. DURMAN
*Sakarya University, Faculty of Engineering, Department of Metallurgy, 54040 Adapazari, Turkey*

S. MURPHY
*Aston University, The Aston Triangle, Birmingham B4 7ET, UK*

The microstructure of ZA27 pressure die-castings was examined by scanning and transmission electron microscopy after ageing for 5 years at ambient temperatures. Solidification began with the formation of compact aluminium-rich $\alpha'$ dendrites and tiny rounded $\alpha'$ particles, followed by the peritectic reaction whereby a zinc-rich $\beta$ phase formed around the edges of the primary phases. The extremely high cooling rate during solidification reduced the extent of the peritectic reaction so that the liquid became highly enriched with zinc and solidification was completed by eutectic formation of $\beta$ and $\eta$ phases, the $\beta$ joining the peritectic $\beta$ and the $\eta$ remaining in the interdendritic regions. On rapid cooling after casting through the eutectoid transformation temperature, the $\beta$ phase decomposed eutectoidally into well-formed lamellae or semi-particulate irregular particles of $\alpha$ and $\eta$, and some lamellar colonies spread into the low-aluminium $\alpha'$-phase cores of the dendrites to form coarse lamellar products. The bulk of the $\alpha'$, however, decomposed into a very fine mixture of zinc-rich phases in an aluminium matrix. These structures are consistent with solidification under conditions of high undercooling. Enclosed within the $\alpha$ constituent of the decomposed peritectic and eutectic $\beta$ phases were small particles of a phase which was identified as the transitional $\alpha'_m$ phase containing 30.2% Al or 14.8% Al, with an f c c crystal structure and lattice parameter (at 14.8% Al) of about 0.395 nm. It had a symmetrical cube/cube orientation relationship with the surrounding $\alpha$ phase. This metastable phase was probably stabilized by copper. Copper became concentrated in the eutectic liquid during the first stages of solidification, and was rejected from the liquid in the form of discrete irregular particles, 1–2 $\mu$m in diameter, during eutectic solidification. After solidification, copper was also rejected from solid solution in the zinc-rich $\eta$ phase in the form of a dense precipitation of small particles of 70–120 nm diameter and 2–3 nm thick. Both of these particles were identified as the metastable c p h $\varepsilon$-phase ($CuZn_4$) with lattice parameters $a = 0.274$ nm, $c = 0.429$ nm, and $c/a = 1.566$.

## 1. Introduction

To meet the need for higher strength and an extended range of service temperatures, the family of ZA alloys, namely ZA8 (Zn–8% Al–1%Cu–0.03%Mg), ZA12 (Zn–12%Al–1%Cu–0.03%Mg) and ZA27 (Zn–27% Al–2%Cu–0.02%Mg) are now well established as a useful supplement to the traditional pressure die-casting zinc-based alloys 3 (Zn–4%Al–0.05%Mg) and 5 (Zn–4%Al–1%Cu–0.05%Mg) (or BS1004 alloys A and B), and are now being used in growing quantities for many small- to medium-sized gravity casting and pressure die-casting applications [1–3]. Of these newer alloys, ZA27 is of particular interest because it attains exceptionally high values of tensile strength of up to about 450 MPa at room temperature, especially in the pressure die-cast form [4, 5]. Unfortunately, it suffers a sharp decline in strength with increased temperature [4, 5], and its use in applications at temperatures above 100 °C is limited owing to its low creep strength [6, 7].

The mechanical properties depend on the microstructure, and in the ZA27 the microstructure is a complex function of the casting process, subsequent cooling rates and ageing reactions. In recent years, although a great deal of work has been carried out to determine the mechanical properties of this alloy in pressure die-cast form at room and elevated temperatures [1–9], only a little work has been done on the relationship between structures and properties [4, 10–15], which is essential if the effects of casting variables and ageing reactions are to be understood. The extreme fineness and complexity of the microstructures found in pressure die-castings have delayed a full understanding of the effects of microstructure in this

0022–2461  

alloy. Thus a necessary first step in understanding the properties of this zinc–aluminium based casting alloy must be the identification of the structures resulting from the solidification process itself and the changes imposed by subsequent solid-state reactions during cooling and ageing at ambient temperatures.

In this work, the metallographic structure of pressure die-cast ZA27 was examined by scanning electron microscopy (SEM) and transmission electron microscopy (TEM) in order to identify the phases present and thus further an understanding of the effects of the alloying elements on structure and properties.

## 2. Experimental procedure

The ZA27 alloy castings used in this work were made from commercial ingot, which was analysed by atomic absorption spectroscopy and found to have the composition Zn–28.5% Al, 2.18% Cu, 0.016% Mg, 0.1% Fe.

An existing commercial die was used to make a typically thin-walled casting approximately 250 mm × 50 mm × 2.18 mm, with additional shallow ribs and bosses. Because of the high aluminium content of ZA27, a cold-chamber pressure die-casting machine was used for the production of the castings. The metallography was carried out on samples cut from the thinner parts of the casting, away from ribs or bosses, so that the structures would be typical of the major parts of such castings. These castings had aged naturally at ambient temperatures for a period of approximately 5 years before examination.

The very fine structures produced by pressure die-casting could not be resolved satisfactorily in the light optical microscope, so the SEM was used to obtain overall views of the metallurgical structures prior to more detailed examination in the transmission electron microscope.

Samples were mounted in conducting bakelite for SEM examination so that sections through the thickness of the plates could be examined. These sections were ground and polished by standard techniques to a 1/4 μm diamond finish and examined in the SEM in the as-polished state using a large-area backscattered electron detector to produce an image. The large atomic number differences between the aluminium-rich and zinc-rich phases allowed the production of medium-resolution images of good contrast in this alloy which displayed the larger scale features of the structures very well.

Thin-foil samples for TEM work were prepared in three stages. Initial thinning of flat samples was carried out by wet-grinding on silicon carbide papers with a grit size of 120 or 160 to produce blanks with a thickness of about 150 μm. Discs of 3 mm diameter were spark-machined from these blanks and further wet-ground on 1200 grit silicon carbide paper using a small jig, down to a thickness of about 100 μm. Final thinning of the discs was carried out by electropolishing in a double-jet Tenupol electropolisher, using a light detector to detect the moment of perforation and automatically stop the thinning process.

A severe problem was encountered initially in obtaining oxide-free specimens, which was ultimately solved by developing a new electrolyte for electropolishing, made up from 30 ml perchloric acid ($d = 1.54\ \mathrm{g\,ml^{-1}}$), 250 ml 2-butoxyethanol and 700 ml ethanol, cooled to sub-zero temperatures with liquid nitrogen. Good results were obtained using a current density of 0.25–0.28 $\mathrm{A\,cm^{-2}}$ at a temperature in the range $-20$ to $-30\,^{\circ}\mathrm{C}$.

The thin foils were examined using Jeol and Philips transmission electron microscopes, most of the work being carried out in a Philips EM 400T instrument equipped with scanning transmission electron microscopy (STEM) and a quantitative energy-dispersive spectroscopy (EDS) analytical system, at 100 keV. Conventional TEM was used to produce high-resolution images and selected-area diffraction patterns (SADP), and convergent-beam diffraction (CBDP) was used to obtain crystallographical information from small phases. The STEM mode of operation was used to obtain a highly focused beam of small diameter in order to determine the chemical compositions of small phases from their characteristic X-ray emissions. Analyses were carried out on thin parts of the foils to minimize errors due to particle/matrix overlap. A special beryllium sample holder was used for analytical work to cut down spectral interferences from that source.

X-ray intensities of the characteristic peaks from the elements of interest were obtained by counting for live times of between 200 and 500 s, using interpolated background subtraction, and quantitative analyses were computed from the peak intensities using atomic number corrections only, because the chemically heterogenous structure of the cast material produced large local variations in foil thickness which made full ZAF corrections impractical.

## 3. Results and discussion

### 3.1. Scanning electron microscopy

Contrast in the SEM images depended principally on the mean atomic number of the different phases present, thus aluminium-rich regions were dark in tone, and zinc-rich regions were light in the scanning electron micrographs. Copper-rich phases could not be differentiated from the zinc matrix enclosing them due to their similar atomic numbers.

The as-cast microstructure of ZA27 is shown at low and high magnification in the scanning electron micrographs in Figs 1 and 2. The general view in Fig. 1 showed the fine and heterogenous microstructure of the naturally aged alloy, consisting of a few compact dendrites of aluminium-rich primary α′-phase set in a mass of much smaller rounded primary particles with interdendritic films and pools of eutectic zinc. At higher magnification in Fig. 2, it appeared that the dendrites of α′-phase had decomposed in some parts into coarse, lamellar cellular products, but more frequently into a very fine mixture of zinc-rich phases in an aluminium matrix.

The interdendritic region was made up of a layer of much more zinc-rich fcc β phase, formed on the α′

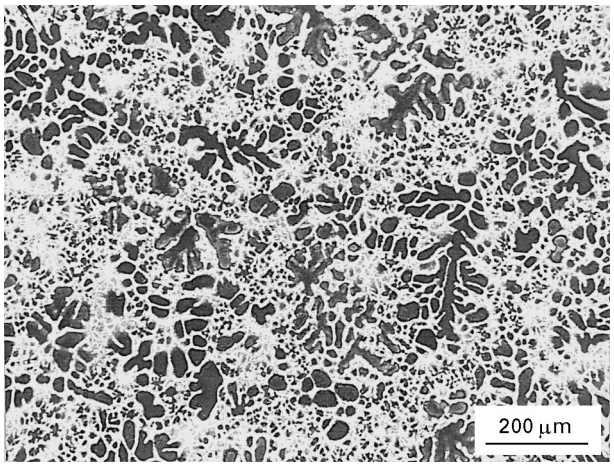


*Figure 1* Scanning electron micrograph in atomic number contrast, showing the general structure of pressure die-cast ZA.27, consisting of fine and heterogenous aluminium-rich α′ dendrites set in a mass of much smaller decomposed peritectic β and eutectic.

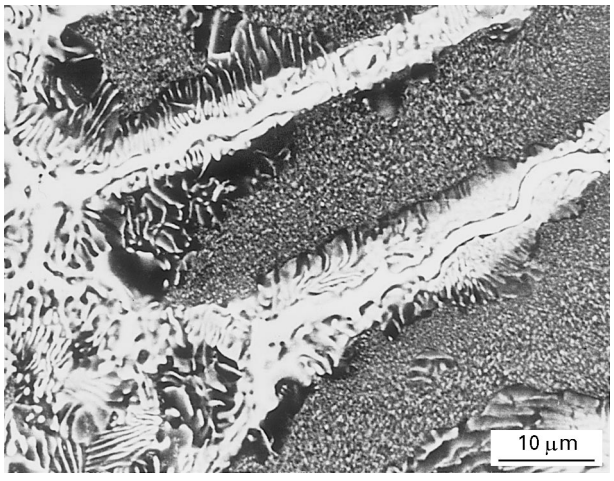


*Figure 2* SEM structure of decomposed primary α′ dendrites surrounded by eutectoidly decomposed peritectic β and interdendritic regions at high magnification.

dendrites by a peritectic reaction of the residual liquid with the first-formed α′ phase and subsequently decomposed eutectoidly into lamellar or irregular particles of α (f c c zinc-rich aluminium solid solution) and η (c p h zinc-rich solid solution), with eutectic zinc occupying the remainder of the space. The relatively small volume fraction of prior β-phase compared with α′ and η in this material was in marked contrast to the proportions found in this same alloy when sand-cast or gravity-cast. This is considered to have come about by partial suppression of the normal peritectic reaction under the high cooling rates associated with pressure die-casting.

## 3.2. Transmission electron microscopy

Using TEM, the alloy showed structures which could be related to those observed by SEM, but with much more detailed information. The contrast mechanism in TEM images of multi-phase structures is different from that in SEM images and depends on preferential thinning, mean atomic number, crystal orientation

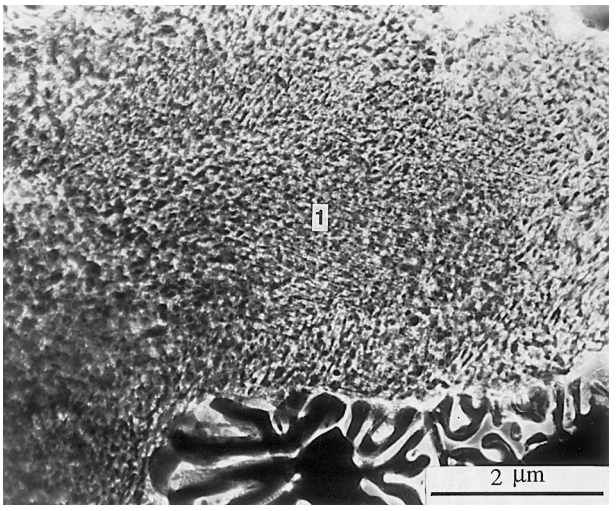


*Figure 3* Conventional TEM BF micrograph of a typical decomposed primary α′ dendrite, showing fine precipitation of zinc in an aluminium matrix in the central portions and coarse cellular products on the surface.

and structure of the different phases present. In general, aluminium-rich phases were light in tone, copper- and zinc-rich precipitated phases were dark, and the zinc-rich matrix phase was of intermediate tone in the transmission electron micrographs.

### *3.2.1. α′-phase decomposition structures*

Fig. 3 shows a bright-field (BF) conventional transmission electron micrograph of a typical complex structure of a decomposed primary α′ dendrite and shows extremely fine-scale precipitation of zinc and aluminium-rich phases in the central portion, and coarse cellular decomposition products on the dendrite surface.

It is now established [16–20] that in Zn–Al alloys with high aluminium contents, the high-temperature α′ phase is transformed into the low-temperature equilibrium phases α + η by two modes of transformation depending on composition, cooling rate and ageing temperature. One is a continuous decomposition of the supersaturated solid solution through the spinodal formation of zones followed by nucleation and growth of a sequence of intermediate, transitional phases with increasing zinc content or size, which can be summed up as follows:

$$\alpha' \rightarrow \alpha + \alpha''_m \rightarrow \alpha + \alpha'_t + \alpha'_m \rightarrow \alpha + \eta$$

where, in addition to previously defined terms, $\alpha''_m$ is a coherent, zinc-rich precipitate with a rhombohedral modification of its f c c structure cell brought about by coherency stresses, $\alpha'_m$ is an intermediate f c c phase with a high zinc content, and $\alpha'_t$ is an intermediate f c c aluminium-rich solid solution in equilibrium with $\alpha'_m$. The other transformation sequence involves a cellular reaction initiated at α′ grain boundaries or inside the grains in which the products are $\alpha'_t + \alpha'_m$, both of which are converted to stable α + η on further ageing.

In the experimental alloy, Fig. 2 shows that the inner part of the dendrite arms had mostly decomposed continuously, but in some regions a cellular

TABLE 1 Mean chemical compositions of the phases in the ZA.27 alloy obtained from EDS analysis (wt%)

| Analysis | Phase | Zn | Al | Cu | Mg |
|---|---|---|---|---|---|
| 1 (Fig. 3) | α′-phase | 30.7 | 64.9 | 3.5 | 0.9 |
| 2 (Fig. 4) | η-matix | 92.1 | 0.9 | 6.7 | 0.3 |
| 3 (Fig. 4) | $\alpha'_m$-phase | 64.6 | 30.2 | 4.8 | 0.4 |
| 4 (Fig. 4) | α-phase | 31.8 | 65.4 | 1.8 | 1.0 |
| 5 (Fig. 6) | $\alpha'_m$-phase | 80.7 | 14.8 | 4.1 | 0.4 |
| 6 (Fig. 6) | α-phase | 27.0 | 70.3 | 1.7 | 1.0 |
| 7 (Fig. 6) | ε-phase | 84.0 | 0.7 | 14.8 | 0.2 |
| 8 (Fig. 6) | η-matrix | 92.6 | 0.9 | 6.3 | 0.1 |

structure had developed from the lamellar products of decomposition of the β-phase coating and grown into the dendrite for a short distance. Because of the higher aluminium content of the dendrite cores, the zinc-rich lamellae became thinner and more widely spaced as the growing cells left the β phase and entered the α′ cores. It appears that the cellular decomposition occurred first, and was halted by the alternative spinodal decomposition which developed before any large-scale penetration into the α′ phase could occur. Thus the continuously decomposed matrix was the dominating decomposition morphology for dendrites as shown in the SEM and TEM images of Figs 2 and 3 respectively. The scale of the equiaxed mixture of the phases in continuously decomposed matrix was extremely fine with an equal average particle diameter of about 90 nm. Quantitative EDS analysis was carried out on the inner parts of the dendrites (e.g. area 1 in Fig. 3) and the results are shown in Table I. These confirmed that these central parts were rich in aluminium, and the development of the two completely different decomposition morphologies had resulted from the differences in composition of the cores of the α′ dendrites compared with their β surfaces.

### 3.2.2. β-phase decomposition structures

According to the Zn–Al binary system, β-phase is unstable below the eutectoid temperature and decomposes into the equilibrium constituents α and η through a eutectoid reaction. In the high-zinc eutectoid or near eutectoid alloys, decomposition of β phase, which is structurally similar to α′ but with higher zinc content, is similar to that of α′ except that the η phase forms together with the $\alpha'_m$ directly from the β phase instead of via the $\alpha'_m$ phase [19–23]. In the experimental alloy, the solid-state transformation of the β-phase into products with different morphologies on cooling below the eutectoid temperature is shown in the bright-field transmission electron micrographs of Figs 4 and 5. In Fig. 4, the lamellar products appeared to have developed from the edge of a mass of interdendritic η and grown into the β, rapidly establishing a regular lamellar morphology of α and η plates with a spacing of about 250 nm. The regular lamellar spacing was achieved most frequently by branching of the existing lamellae, and occasionally by the nucleation and growth of fresh lamellae at the advancing interface inside the β cells, indicating that

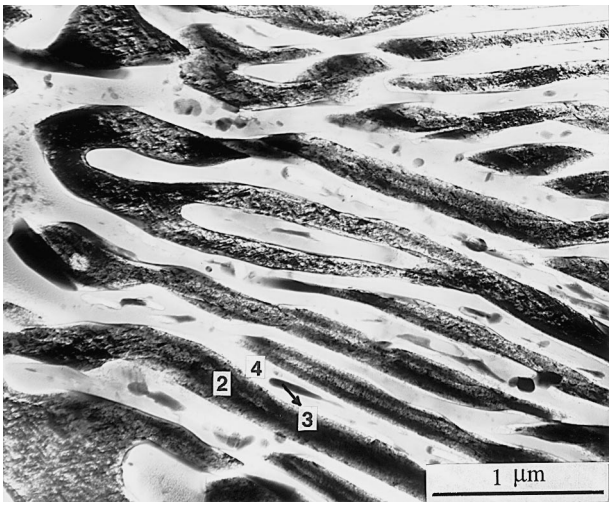


*Figure 4* BF micrograph of lamellar products α + η of eutectoidly decomposed peritectic β with centrally disposed $\alpha'_m$ in the α phase and a dense precipitate of ε-phase in η matrix.

a typical conventional cellular reaction mechanism was operative. An alternative mechanism produced a complex particulate mixture of α and η, together with an irregular suppressed lamellar microstructure. A typical microstructure illustrating the coexistence of both products formed on each side of an interdendritic film of η is shown in Fig. 5. The generally convex shapes of the particles, together with their numerous inter-connections suggested that they were only partially particulate and had formed as complex interwoven tubular structures around the advancing cellular colonies. This change in the decomposition morphology of β-phase in Zn–Al alloys has been reported by many workers [24, 25], and is attributed to the development of internal stress in the untransformed matrix ahead of the moving interface, thereby providing heterogenous sites for the nucleation of the equilibrium phases.

Examination of Figs 4 and 5 showed also that the η phase regions formed by β phase decomposition were occupied by large numbers of small uniformly distributed precipitates forming a very high-density dispersion throughout the matrix (e.g. area 2 in Fig. 4). The α phase showed no similar precipitate, although small rounded or elongated particles, some 30–200 nm in diameter, were present within the α phase constituent of the cellular and mixed products of β transformation, (e.g. particle 3 in Fig. 4). These often exhibited darker contrast than the surrounding α matrix, and with distinct boundaries. In order to identify these precipitates in η and α, quantitative EDS analysis, using the STEM mode to produce a highly focused beam where necessary, was carried out on the three phases marked in Fig. 4: the η matrix (2) which included the fine precipitates, the particle (3) embedded in the α matrix, and the α matrix (4). At least ten analyses were carried out on different examples of each phase, and the mean results are shown in Table I. In these and other analyses shown in Table I, the aluminium to zinc ratio is considered to be correct, but the copper and magnesium contents are slightly

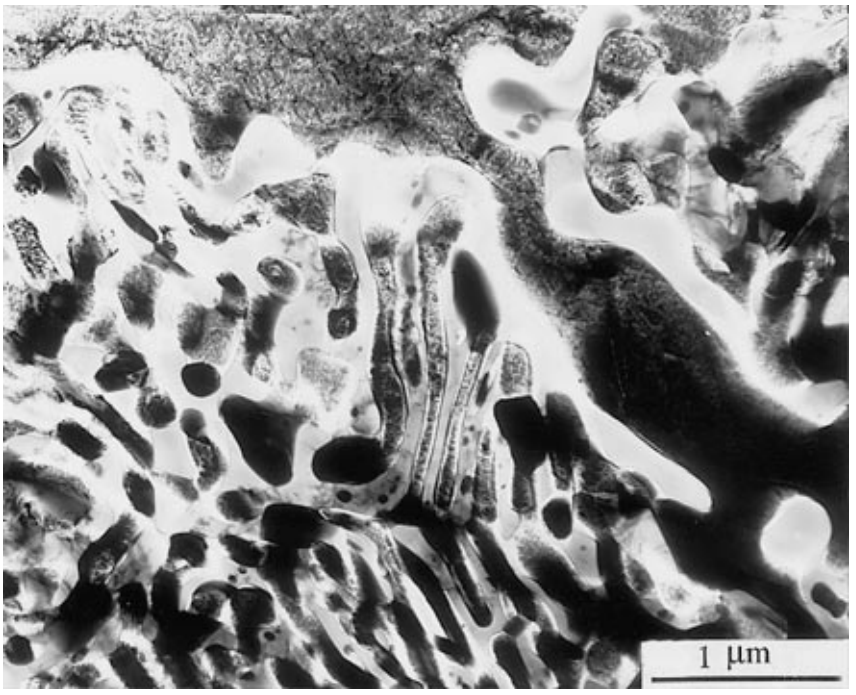


*Figure 5* BF micrograph of complex microstructure of decomposed peritectic β, showing the coexistence of particulate and suppressed lamellar products with $\alpha'_m$ and ε precipitates in α and η matrix, respectively.

and much too high, respectively, probably due to a surface film formed on the thin foils during electropolishing and to poor background estimation of the analytical programme used. Taking these reservations into account, the results shown in Table I indicated that region 2, with the higher than average copper content of 6.7%, was a zinc solid solution of equilibrium composition containing fine copper-rich precipitates; the α phase (4) was a solid solution of near-equilibrium composition except for a higher zinc content, but the internal particle (3) embedded in the α matrix was a zinc-rich phase containing 30.2% aluminium which did not correspond with any phase of the Zn/Al/Cu system stable at ambient temperatures. Both of these copper- and zinc-rich precipitate phases were also found in decomposed eutectic counterparts of η and α and were identified as metastable transitional phases, as discussed in detail in the following sections.

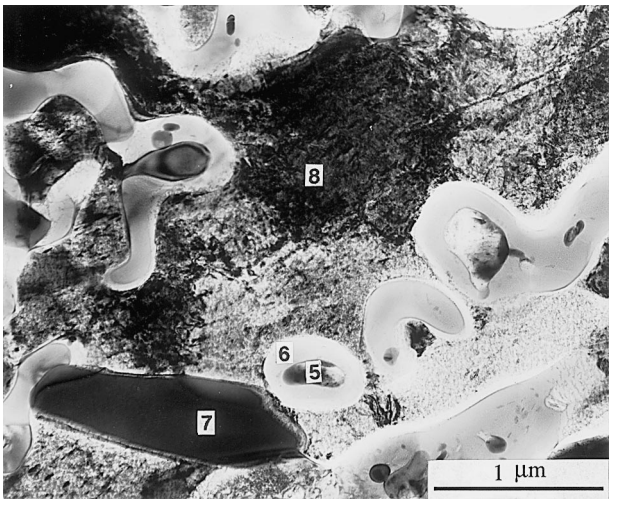


*Figure 6* BF micrograph of the eutectic region, showing the embedded $\alpha'_m$ particles in eutectic α, and a larger ε-phase particle in the interdendritic region. Fine precipitates of ε-phase are also visible in high densities throughout the eutectic η matrix.

### 3.2.3. Eutectic solidification structures

Fig. 6 is a BF image of a typical interdendritic area observed in the experimental alloy, formed mainly by eutectic solidification and partly by β phase decomposition. At the eutectic solidification point, the eutectic liquid existed as narrow films separating β-coated α′ primaries, and on solidification the β product from the eutectic reaction had grown on to the adjacent β, leaving solid η phase as a thin film between the primaries. Although crystallographically continuous, the two β layers must have differed in composition, as the Zn/Al phase diagram shows nearly 30% Al in peritectic β and 19% Al in eutectic β. On cooling through the eutectoid temperature, β must decompose into the stable products α and η, and Fig. 6 showed that the former β plates had transformed into small plates or rows of spheroidal or tubular aluminium-rich α particles, embedded in an η matrix which was continuous with the η phase of the eutectic. The varying contrast in the η phase in this micrograph indicated that it was polycrystalline with a grain size of about 1–3 μm. It was also apparent that in the middle of the α particles, there were rounded or elongated particles similar to those found in the α product of the peritectic β decomposition, but larger in size, i.e. about 100–400 nm diameter (e.g. particle 5 in Fig. 6). Quantitative EDS analysis was carried out on different examples of these particles and the α matrices enclosing them (e.g. area 6 in Fig. 6), and the mean results are shown in Table I. These results revealed that the α matrices had near equilibrium compositions, but the inner particles were a zinc-rich phase containing

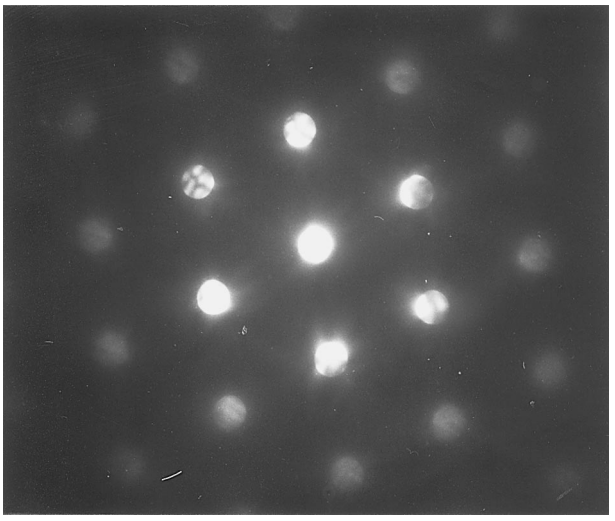

*Figure 7* CBDP showing ⟨1 1 0⟩ fcc zone from metastable $\alpha'_m$ phase embedded in eutectic α.

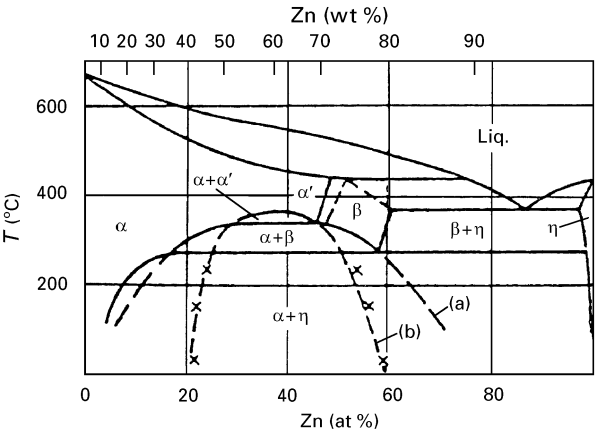


*Figure 8* Zn–Al phase diagram, showing the position of the metastable miscibility gap and composition of the metastable phases. (a) extrapolation of the β solubility curve to ambient temperatures, (b) extrapolation of the α/α′ boundary of the monotectoid two-phase field to ambient temperatures (from Toldin *et al.* [22]).

14.8% aluminium which did not correspond to any phase of the Zn/Al/Cu system stable at ambient temperatures. The α phase was of approximately the same composition as that in the decomposed peritectic β, but the inner particles had a lower aluminium content and a higher copper content.

Convergent-beam diffraction was used for the identification of this unknown phase in the eutectic and an electron diffraction pattern is shown in Fig. 7 which was indexed as a ⟨1 1 0⟩ zone of an fcc structure. Using the same technique, a diffraction pattern was also obtained from the α-phase immediately adjacent to this unknown phase, which gave an identical zone with the reflections parallel to the corresponding ones in the unknown phase but with different reciprocal lattice spacings, indicating that the two crystal lattices were exactly parallel, i.e that the two phases had the cube/cube orientation relationship, but had different lattice parameters. From the known zinc content of 27% in the matrix α, its lattice parameter was estimated as $a = 0.4024$ nm, and this was used as a calibration to determine the lattice parameter of the unknown fcc phase as $a = 0.395$ nm. The fcc structure cell with smaller lattice parameter and aluminium content of 14.8% identify this phase as the transitional $\alpha'_m$ phase frequently found in binary zinc/aluminium alloys with high aluminium contents on quench-ageing [16–23] and more recently in a ZA27 alloy during natural ageing after quenching [13] and in a pressure die-cast ZA8 alloy after the same period of natural ageing time as the alloy studied in this work [26].

In the Al/Zn phase diagram, two metastable miscibility gaps have been proposed, which indicate the possible compositions of such metastable products [22, 27], and this is shown, with the phase fields relabelled according to our convention, in Fig. 8. On this phase diagram, extrapolation of the β solubility curve to near ambient temperature indicates that the expected composition of the high-zinc metastable phase would lie very close to the measured composition of the transitional phase found in the eutectic in this work. The composition of the α matrix in metastable equilibrium with this phase in the eutectic also corresponds approximately to the other boundary of the metastable two-phase field in the diagram. Thus it is possible that a eutectic β phase with an aluminium content of approximately 19% could form transitional phases $\alpha'_t$ and $\alpha'_m$ with fcc structures and aluminium contents of about 70 and 15 wt %, respectively.

On the other hand, extrapolation of the α/α′ boundary of the monotectoid two-phase field of Fig. 8 to near-ambient temperatures indicates that transitional phases $\alpha'_t$ and $\alpha'_m$ would form with compositions very near to the experimental values of 65.4 and 30.2 wt% Al measured in this work for α and $\alpha'_m$, respectively, in the decomposed peritectic β. Thus the higher aluminium content of the $\alpha'_m$ found in the α constituent of the original peritectic β, may be due to the higher aluminium content of that phase.

The transitional $\alpha'_m$ phase in binary Zn/Al alloys exists only briefly during ageing after quenching, yet it was found in considerable amounts in this pressure die-cast alloy which had been aged at ambient temperatures for over 5 years, suggesting that copper or magnesium must have had a strong stabilizing effect on $\alpha'_m$. The absence of this phase in pressure die-cast alloy 3 which had a similar magnesium content to ZA27 but contained no copper, after a similar period of ageing [28], suggests that copper must have stabilized the $\alpha'_m$ phase, whereas magnesium had little or no effect.

### 3.2.4. Precipitation of copper

Examination of the eutectic in Fig. 6 showed also that the η constituent of the eutectic contained two types of precipitate phases with distinctly different sizes and morphologies. One was in the form of discrete, acicular particles varying from 1–2 μm in diameter (e.g. particle 7 in Fig. 6), distributed irregularly in the interdendritic channels, the second type was a fine, uniformly distributed copious precipitate in the zinc matrix (area 8 in Fig. 6) similar to those copper-rich precipitates found in the η constituent of the decomposed peritectic β phase. Other examinations

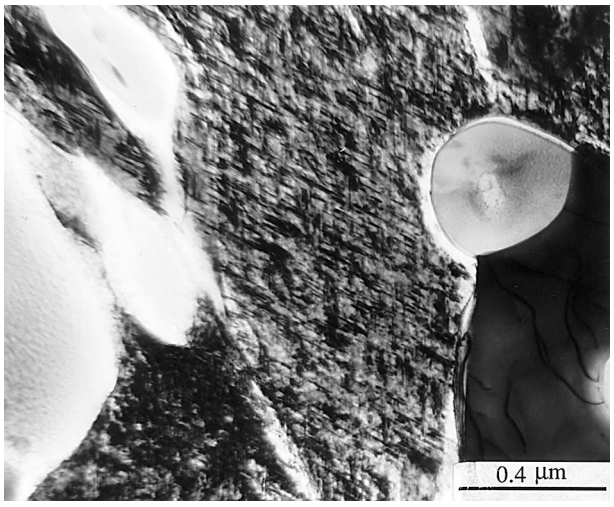


*Figure 9* BF micrograph of eutectic region in Fig. 6 showing dense, uniformly distributed precipitates of ε-phase in the η matrix.

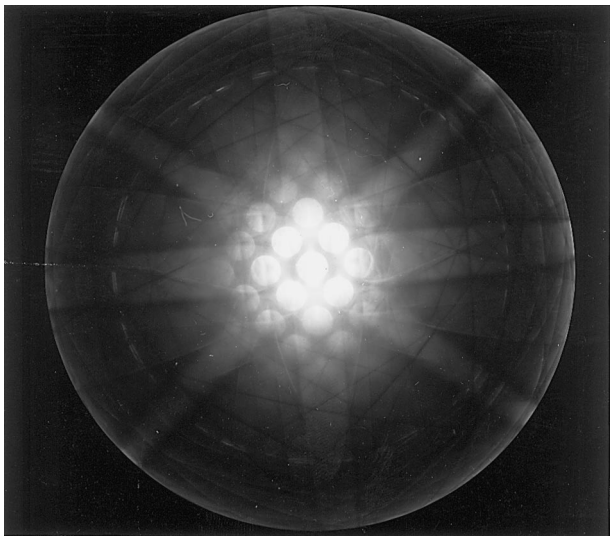

*Figure 10* CBDP from the large ε-particle in Fig. 6, showing the h c p symmetry of $\langle 0\,\bar{1}\,1\,1\rangle$ zone.

confirmed that all the η phase in the interdendritic area contained these fine precipitates and when they were brought into contrast at high magnification, as for example in Fig. 9, it was apparent that at least two families of these precipitate particles 70–120 nm in length or diameter and 2–3 nm in thickness were present in the matrix, each with its own growth direction or habit plane.

Identification of both of these precipitates was attempted by using EDS chemical analysis, and crystallographic analysis through CBDPs and SADPs. The results of quantitative EDS analyses carried out on different examples of the large individual particles such as particle 7 in Fig. 6, are shown in Table I. These results indicated that these particles were a zinc-rich phase containing approximately 15% Cu and 1% Al, which closely corresponded to the equilibrium composition of the ε-phase ($CuZn_4$) of the Cu/Zn/Al system, stable at temperatures above about 280 °C [29]. CBDPs obtained from these particles, an example of which from a $\langle 0\,\bar{1}\,1\,1\rangle$ h c p zone is shown in Fig. 10, also confirmed that these particles were indeed ε-phase with lattice parameters $a = 0.274$ nm, $c = 0.429$ nm, and $c/a = 1.567$. These discrete ε-particles had formed in the copper-enriched liquid when the eutectic solidification took place.

Chemical analysis of individual fine precipitates of the second type was not possible owing to the fine scale of precipitation and thus much particle/matrix overlapping, even though the STEM mode was used to produce a finely focused electron beam, but EDS analyses of the η matrix in different areas of the eutectic (e.g. area 8 in Fig. 6) which included the fine precipitates, showed that the aluminium content of this region was only about 1%, but the copper content gave a consistent mean value of 6.3% from all analyses (Table I).

The high overall copper contents of the η regions together with the known low solubility of copper in η at ambient temperatures [30], suggested that these precipitates were also a copper-rich phase formed on cooling after casting. To identify these precipitates, a large number of CTEM SADPs from the eutectic η phase and the η constituent of the decomposed β phase were examined for subsidiary reflections, but only $\langle 1\,\bar{2}\,1\,0\rangle_\eta$ and $\langle 1\,0\,\bar{1}\,0\rangle_\eta$ zones showed minor reflections which could not be associated with epitaxial surface oxide. Fig. 11a shows an example of a $\langle 1\,\bar{2}\,1\,0\rangle_\eta$ zone from the eutectic matrix with two sets of streaked reflections from the precipitate. The indexing of this diffraction pattern is shown in Fig. 11b, where for clarity only one of the two sets of streaked h c p zone reflections is indexed, and this showed that all three zones were c p h, but the $c/a$ ratio of the subsidiary crystals differed from that of the matrix, and the $\{0\,0\,0\,1\}$ planes were not exactly parallel. The $c/a$ ratio of the η matrix corresponded closely to that of zinc with about 1% dissolved copper [31], and in view of the chemical analysis showing very little aluminium in the matrix, a calibration factor could be obtained from the zinc reflections which allowed the interplanar spacings of the subsidiary phase to be determined. The phase was then identified as the ε-phase ($CuZn_4$), with the same lattice parameters as those given above. These precipitate particles were identical in their morphology to those found in an earlier study [32] of pressure die-cast ZA8 alloy after the same period of ageing as the alloy studied in this work, where their orientationship with the parent η matrix and habit plane were precisely determined and discussed in detail. However, compared to the ZA8 alloy, the precipitation density was found to be much higher in ZA27. This must be due to the higher copper content and reduced volume fraction of η phase regions in ZA27 alloy.

It is, however, significant to note that the ε-phase found in large quantities in this experimental alloy is not stable at temperatures below 280 °C, and must eventually be replaced by the equilibrium T′ phase [29, 33], but no diffraction evidence was found for the T′ phase even after such a prolonged period of natural ageing. The T′ phase contains 12% Zn, 58% Cu and 30% Al [29], so because the ε-phase was found to be dispersed in η, which contains very little dissolved aluminium, conversion of ε-phase to T′ phase must

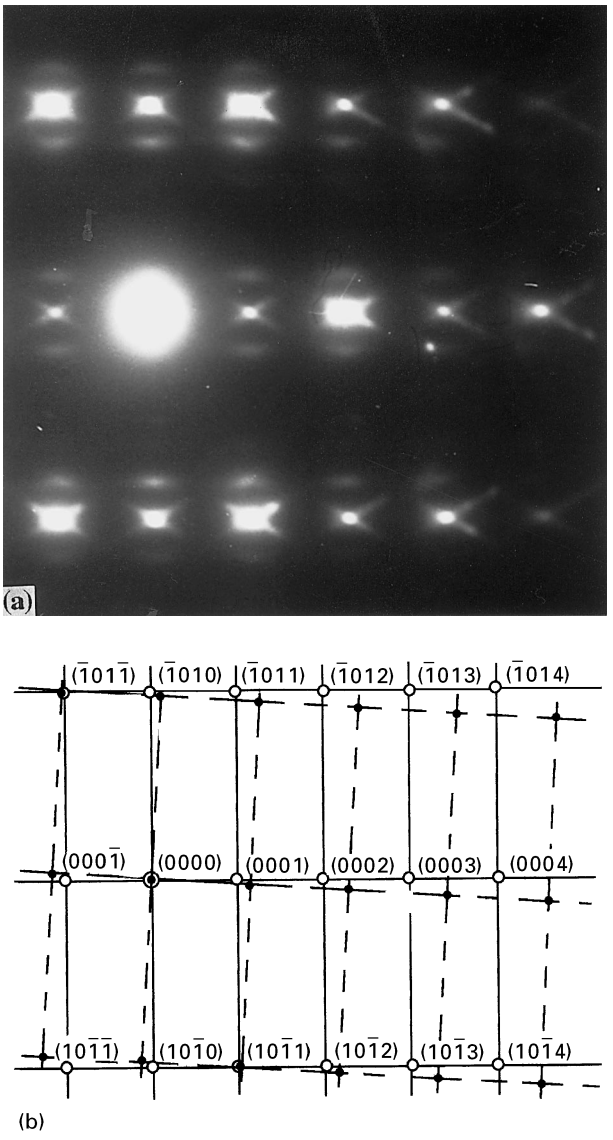


*Figure 11* (a) SADP from the eutectic η matrix in Fig. 9, consisting of a $\langle 1\bar{2}10\rangle_{\eta}$ zone and two sets of streaked precipitate reflections. (b) Indexing of (a), streaked reflections from two $\langle 1\bar{2}10\rangle_{\varepsilon}$ zones; only one set is labelled for clarity. (○) $\langle 1\bar{2}10\rangle_{\eta}$, (●) $\langle 1\bar{2}10\rangle_{\varepsilon}$.

involve either migration of aluminium into the η, or re-solution of ε and diffusion of copper through the η to the α-phase where a T′ phase could nucleate. The similar crystal structures and small lattice misfits between ε-phase and the zinc matrix, combined with long diffusion paths are considered to be the reasons for the long-term metastability of the ε-phase in this alloy.

Copper is known to improve both the strength and creep resistance of Zn–Al–Cu alloys. The identification of a dense dispersion of very small, highly persistent particles of the metastable copper-rich ε-phase in the η matrix, strongly indicates that the improvements are due to the effects of this precipitate on the strength on the η phase, which is the dominant phase in zinc–aluminium-based commercial alloys. It was therefore shown that among the ZA alloys, ZA8 alloy with composition near to the eutectic composition and containing 1% copper had a substantially better creep resistance than the other alloys in the family [6,7].

The bigger, discrete ε-phase particles found irregularly distributed in the interdendritic channels, which are thought to form almost simultaneously with (β + η) eutectic from the copper- and zinc-rich eutectic liquid, should not have such a strong effect on the mechanical properties, but would probably give a slight improvement. Indeed, in a recent work [34] it was shown that in a ZA27 alloy, copper additions of up to 1% had a profound effect in increasing the creep resistance of the alloy, but increasing the copper content from 1% to 2% produced very little further creep resistance.

### 3.2.5. The concentration of magnesium

The effect of magnesium on the mechanical properties is known to be beneficial even at the very low level used in this alloy, but the effects of this element on the microstructure were not directly apparent and no magnesium-rich compounds were detected. Table I shows EDS analytical results in which the magnesium contents of all phases analysed were too high to be credible, because in the experimental alloy as a whole the average magnesium content was less than 0.02 wt%. However, in all the analyses carried out in this work the magnesium content was consistent, with almost the same amount in the zinc-rich phases, but much higher amounts in aluminium-rich α phases. Thus it is probable that magnesium was concentrated preferentially into the α phase, but the actual concentrations are not known and its role remains unclear.

## 4. Conclusions

1. Zinc-alloy pressure die-castings of ZA27 were examined after ageing for 5 years at ambient temperatures. The cast alloy had initially solidified to form primary aluminium-rich α′ dendrites and particles with a coating of peritectic β, set in a eutectic zinc matrix. These structures are consistent with solidification under conditions of high undercooling.

2. The high-temperature α′ phase forming the primary dendrites subsequently decomposed in some parts into coarse, lamellar cellular products, and more frequently in others into a fine mixture of zinc-rich phases in an aluminium matrix, whereas β phase decomposed eutectoidly to form semi-particulate irregular particles of α and β or well-formed lamellar products with an interlamellar spacing of about 250 nm.

3. The β-decomposition products were identified as α and η phases with average compositions which corresponded closely to the equilibrium compositions at ambient temperatures, except that copper was preferentially segregated into the η-phase. A third phase located at the centres of the α-phase particles or plates of both the decomposed peritectic and eutectic β was the metastable fcc phase $\alpha'_m$ found in quench-aged zinc–aluminium alloys.

4. The $\alpha'_m$ phase enclosed in the α constituent of decomposed peritectic β contained 30.2% Al, and that in eutectic α contained 14.8% Al. The lattice parameter of the fcc crystal structure was estimated as

about 0.395 nm at 14.8% Al, and it had adopted a symmetrical cube/cube orientation relationship with the surrounding α phase. This metastable phase had probably been stabilized by copper.

5. Copper had concentrated preferentially in the eutectic liquid during solidification, and on cooling through the eutectic temperature discrete irregular particles, 1–2 μm in diameter, had formed in the interdendritic regions, which were identified as the c p h metastable ε-phase ($CuZn_4$). Most of the remaining copper was dissolved in the η phase formed on solidification or by solid-state transformation, and this had been rejected from solid solution during cooling after casting in the form of a dense precipitation of small particles 70–120 nm in length or diameter and 2–3 nm in thickness. These particles were identified as ε-phase with lattice parameters $a = 0.274$ nm, $c = 0.429$ nm, and $c/a = 1.566$.

6. Although thermodynamically unstable at ambient temperatures in ZA27, the fine dispersion of metastable ε-phase particles in the η matrix was still present after ageing for 5 years after casting, and this persistent fine dispersion is thought to be responsible for most of the known improvements in mechanical properties brought about by the addition of copper to zinc-based alloys.

## Acknowledgements

This work was carried out in the Department of Mechanical and Electrical Engineering at Aston University; the Head of Department, Dr J.E.T. Penny, is thanked for the provision of facilities. The majority of the TEM work was carried out using the instruments at the University of Birmingham whose help in the provision of high-resolution TEM facilities is gratefully acknowledged. The authors are also grateful for the financial support of the Republic of Turkey for one of the authors and the generous support of Pasminco Europe Ltd (now Britannia Zinc Ltd) in furthering this work.

## References

1. E. GERVAIS, H. LEVERT and M. BESS, *Trans. AFS* **88** (1980) 183.
2. E. GERVAIS, *CIM Bulletin*, **80** (1987) 67.
3. E. J. KUBEL, *Adv. Mater. Process.* **7** (1987) 51.
4. S. MURPHY, M. DURMAN and J. HILL, in "12th International Pressure Die-caster Conference, Florence, Italy (1987).
5. C. A. LOONG, in SDCE 14th International Die-casting Congress and Exposition, Paper No. G-T87-027, Toronto, Ontario, Canada, May 11–14, 1987. Edited by the Society of Die-casting Engineers Inc., River Grove, USA (1987).
6. S. MURPHY, M. DURMAN and J. HILL, *Z. Metallkde* **79** (1988) 243.
7. M. DURMAN and S. MURPHY, *ibid.* **82** (1991) p. 129.
8. F. E. GOODWIN and A. L. PONIKVAR, "Engineering Properties of Zinc Alloys", 3rd Edn, revised (International Lead–Zinc Research Organisation Inc., North Carolina, USA, 1989).
9. R. J. BARNHURST, "Zinc and Zinc Alloys", in ASM Handbook (formerly 10th Edn, Metals Handbook) edited by ASM International Handbook Committee, Vol. 2 (ASM, Ohio, USA, 1992) p. 527.
10. "ASM Handbook" (formerly 9th Edn, "Metals Handbook") edited by ASM International Handbook Committee, Vol. 9 (ASM, Ohio, USA, 1992) p. 418.
11. J. LECOMTE-BECKERS, L. TERZIEV, J. WEGRIA and T. GREDAY, *Phys. Stat. Sol.* (A), **116** (1989) 521.
12. L. LAMBERIGTS, G. WALMAG and D. COUTSOURADIS, in "Proceedings of the 3rd International Conference on Solidification Processes", Sheffield, UK, (Institute of Metals, London, 1988) p. 281.
13. W. HONGMIN, C. QUANDE, W. YIGUI and Z. YUANGENG, *J. Mater. Sci.* **27** (1992) 1212.
14. P. RACHEV, L. TERZIEV, J. LECOMTE-BECKERS and J. WEGRIA, *Acta Metall.* **39** (1991) 2177.
15. H. LEHUY and G. L'ESPERANCE, *J. Mater. Sci.* **26** (1991) 559.
16. R. D. GARWOOD, A. L. DAVIES and G. L. RICHARDS, *J. Inst. Metals* **88** (1959-60) 375.
17. M. SIMERSKA and V. SYNECEK, *Acta Metall.* **15** (1967) 223.
18. G. J. C. CARPENTER and R. D. GARWOOD, *Metal Sci. J.* **1** (1967) 202.
19. A. KURUPKOWSKI, R. CIACH and J. KROL, *Bull. Acad. Pol. Sci.* **15** (1967) 1975.
20. V. A. TOLDIN, G. V. KLESHCHEV, D. V. SHUMILOV and A. J. SHEYNKMAN, *Fiz. Metal. Metalloved.* **40** (1975) 1223.
21. V. A. TOLDIN, A. A. BURYKIN and G. V. KLESHCHEV, *Phys. Met. Metall.* **40** (1978) 97.
22. *Idem*, *ibid.* **51** (1981) 116
23. R. CIACH, J. KROL and K. WEGRZYN-TSAIOR, *Bull. Acad. Pol. Sci.* **17** (1969) p. 371.
24. M. VIJAYALAKSHMI, V. SEETHARAMAN and V. S. RAGHUNATHAN, *Mater. Sci. Eng.* **52** (1982) 249.
25. *Idem*, *Acta Metall.* **30** (1982) 1147.
26. M. DURMAN and S. MURPHY, *J. Mater Sci.* **27** (1992) 3215.
27. A. KURUPKOWSKI, R. CIACH and J. KROL, *Bull. Acad. Pol. Sci.* **15** (1967) 25.
28. M. DURMAN, K. SAWALHA and S. MURPHY, *Mater. Sci. Eng. A***130** (1990) 247.
29. S. MURPHY, *Z. Metallkde* **71** (1980) p. 96.
30. M. HANSEN and K. ANDERKO, "Constitution of Binary Alloys", 2nd edn (MacGraw-Hill, New York, 1958) p. 651.
31. W. B. PEARSON, "A Handbook of Lattice Spacings and Structures of Metals and Alloys", Vol. 2 (Pergamon Press, Oxford, 1967).
32. M. DURMAN and S. MURPHY, *Acta Metall.* **39** (1991) 2235.
33. S. MURPHY, *Metals Sci.* **9** (1975) 163.
34. M. DURMAN and S. MURPHY, Recent Advances in Science, Technology and Applications of Zn-Al Alloys, Proceedings of the 3rd. International Conference on Zn-Al Alloys, Mexico, March, 1994, edited by G. Torres-Villasenar, Y. Zhu and C. Pina-Barba (Universidad Nacional Autónoma de Mexico, Mexico, 1994) p. 59.

*Received 21 August 1995*
*and accepted 21 May 1996*